EPJ Web of Conferences **109**, 04005 (2016)
DOI: 10.1051/epjconf/201610904005

Experimental investigation of the ^{30}S(α, p) thermonuclear reaction in x-ray bursts

D. Kahl[1,a], A. A. Chen[2], S. Kubono[1,3,4], H. Yamaguchi[1], D. N. Binh[1], J. Chen[2], S. Cherubini[6], N. N. Duy[5], T. Hashimoto[1], S. Hayakawa[1], N. Iwasa[7], H. S. Jung[8], S. Kato[9], Y. K. Kwon[8], S. Nishimura[3], S. Ota[1], K. Setoodehnia[2], T. Teranishi[10], H. Tokieda[1], T. Yamada[7], C. C. Yun[8], and L. Y. Zhang[4]

[1] *Center for Nuclear Study, Graduate School of Science, the University of Tokyo, Japan*
[2] *Department of Physics & Astronomy, McMaster University, Canada*
[3] *RIKEN Nishina Center, RIKEN (The Institute of Physical and Chemical Research), Japan*
[4] *Institute of Modern Physics, Chinese Academy of Sciences, China*
[5] *Institute of Physics, Vietnam*
[6] *Department of Physics, University of Catania & INFN, Italy*
[7] *Department of Physics, Tohoku University, Japan*
[8] *Department of Physics, Chung-Ang University, Korea*
[9] *Department of Physics, Yamagata University, Japan*
[10] *Department of Physics, Kyushu University, Japan*

Abstract. We performed the first measurement of ^{30}S+α resonant elastic scattering to experimentally examine the ^{30}S(α, p) stellar reaction rate in type I x-ray bursts. These bursts are the most frequent thermonuclear explosions in the galaxy, resulting from thermonuclear runaway on the surface of accreting neutron star binaries. The ^{30}S(α, p) reaction plays a critical role in burst models, yet very little is known about the compound nucleus ^{34}Ar at these energies nor the reaction rate itself. We performed a measurement of alpha elastic scattering with a radioactive beam of ^{30}S to experimentally probe the entrance channel. Utilizing a gaseous active target system and silicon detector array, we extracted the excitation function from 1.8 to 5.5 MeV near 160° in the center-of-mass frame. The experimental data were analyzed with an *R*-Matrix calculation, and we discovered several new resonances and extracted their quantum properties (resonance energy, width, spin, and parity). Finally, we calculated the narrow resonant thermonuclear reaction rate of ^{30}S(α, p) for these new resonances.

1 Introduction

Type I x-ray bursters (XRBs) are a class of astronomical objects observed to increase in luminosity by factors of roughly 10^{1-3} for a short period of time (tens of seconds) with the photon flux peaking in the x-ray. The sources of such emission repeat these outbursts typically on timescales of hours to days, allowing for the extensive study of the burst morphology of individual XRBs. XRBs are modelled

[a] e-mail: daid@cns.s.u-tokyo.ac.jp

very successfully as neutron star binaries accreting material rich in hydrogen and helium from a low-mass companion. The accretion mechanism causes the formation of an electron-degenerate envelope around the neutron star, where the thin-shell instability triggers a runaway thermonuclear explosion, which we observe as an x-ray burst.

The sharp rise of the x-ray fluence is largely due to explosive helium burning, which in a mixed hydrogen and helium shell is a series of $(\alpha, \mathrm{p})(\mathrm{p}, \gamma)$ reactions on oxygen seed nuclei near the proton drip line, called the αp-process [1]. In XRBs, where the nuclear reaction network includes hundreds of species and thousands of nuclear transmutations, it is actually only a small subset of these nuclear transmutations which need to be known precisely, as they make a predominant contribution to the nuclear trajectory to higher mass and energy generation. The $^{30}\mathrm{S}(\alpha, \mathrm{p})$ reaction is identified as one such important reaction, contributing more than 5% to the total energy generation [2], influencing the neutron star crustal composition [3] relevant to compositional inertia [4], moving material away from the ^{30}S waiting point [5], and possibly accounting for double-peaked XRBs [6].

Unfortunately, there is very little experimental information on the $^{30}\mathrm{S}(\alpha, \mathrm{p})$ stellar reaction rate nor the structure of ^{34}Ar above the alpha-threshold, essentially limited to a preliminary report on a transfer reaction study of the compound nucleus ^{34}Ar at high excitation energy [7] and a time-reversal study [8]. The present work is the first experimental investigation using the entrance channel $^{30}\mathrm{S}+\alpha$.

2 Experiment

We performed a measurement of ^{30}S+alpha resonant elastic scattering using the thick-target inverse-kinematics technique [9]. The radioactive ^{30}S beam was produced in-flight via the $^{3}\mathrm{He}(^{28}\mathrm{Si}, ^{30}\mathrm{S})\mathrm{n}$ reaction using the Center for Nuclear Study (CNS) low-energy radioactive ion beam separator (CRIB) [10, 11], where we bombarded a cryogenically-cooled gas cell [12] of ^{3}He at 1.72 mg $\cdot$ cm^{-2} with a ^{28}Si beam at 7.3 MeV/u [13]. The ^{30}S beam arrived on target at 1.6 MeV/u, an average of 30% purity, and with an intensity of 10^4 particles per second.

The beam was tracked by two parallel plate avalanche counters (PPACs) [14] which served as beamline monitors, before impinging on a newly developed active target system. The active target system was sealed with a 7.4 μm Kapton foil and filled with 194 Torr ($\approx \frac{1}{4}$ atm) of 90% He and 10% CO_2, comprised of a field cage, a low-gain region surrounded on three sides by a high-gain region and silicon strip detector telescopes. Between the field cage and the backgammon-type readout pads were gas electron multiplier (GEM) foils to control the specific gain. A portion of the detector schematic and the present method of determining the scattering point is shown in Figure 1; further details of the present active target system can be found in [15]. Each portion of the active target can measure the three-dimensional position of ionizing radiation (using pad number, charge comparison on two opposite sides, and electron drift time, respectively) as well as the local energy loss ΔE (total charge collected on one pad).

We measured scattered alpha particles over laboratory angles of $10^\circ \leq \theta_{\mathrm{lab}} \leq 25^\circ$ and center-of-mass energies from 1.8 MeV $\leq E_{\mathrm{cm}} \leq$ 5.5 MeV.

3 Results

We determined the center-of-mass energy event-by-event for scattered alpha particles to produce the $^{30}\mathrm{S}+\alpha$ spectrum. The center-of-mass excitation function is defined as

$$\frac{d\sigma}{d\Omega} = \frac{Y_\alpha S(E_{\mathrm{beam}})}{I_{\mathrm{beam}} n \Delta E \Delta\Omega} \frac{m_\alpha}{m_\alpha + m_{^{30}\mathrm{S}}}, \tag{1}$$

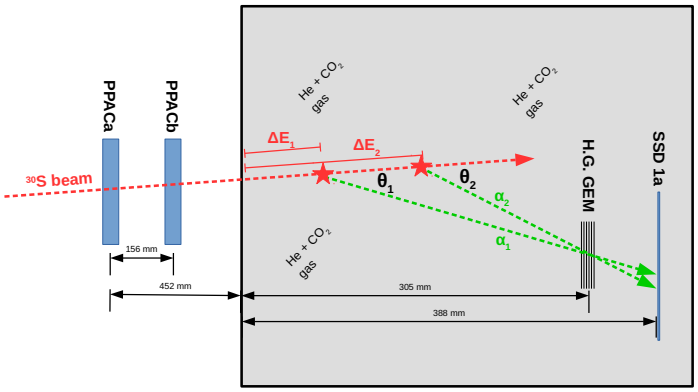

Figure 1. Schematic view of a portion of the experimental setup and the scattering point determination; it is not drawn to scale. In the cartoon, two distinct scattering positions are depicted, where the geometrical measurements of the detectors are identical. Two beamline monitors (PPACa and PPACb), one high-gain GEM (H.G. GEM) and one silicon detector (SSD) are shown. It is clear the energy loss of the ^{30}S beam $\Delta E_1 \neq \Delta E_2$ (changing the center-of-mass energy), as well as the laboratory alpha scattering angle $\theta_1 \neq \theta_2$, and thus the scattering energy differs, hence the residual alpha particle energy measurement by the SSD cannot be the same. By considering all possible scattering positions and comparing the calculated residual alpha particle energy with the measurement, a unique solution is found within the uncertainties.

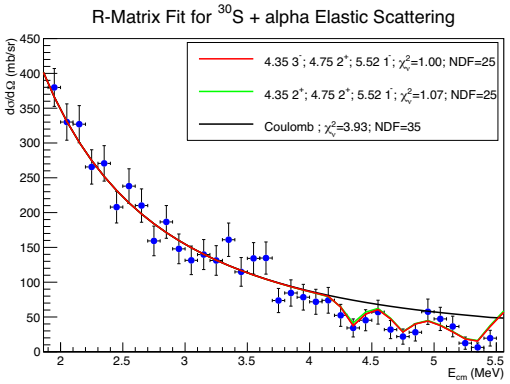

Figure 2. ^{30}S+α elastic scattering excitation function. The energy range displayed is the entire set of continuous data in the raw excitation function, except at the lower energy side where the plot is terminated at the point where all the α particles can no longer reach the detector from stopping in the fill gas. The bumps observed around 3.5 MeV correspond to a region of large alpha-background which are a component of the cocktail beam; even introducing resonances with the Wigner limit do not make a noticeable change to the *R*-Matrix curve in this region. Three resonant-like structures are seen between $4 < E_{\rm cm} < 5.5$ MeV.

where Y_α is the yield of alpha particles at each energy bin, $S(E_{\rm beam})$ is the stopping power of He+CO_2 for ^{30}S, $I_{^{30}\rm S}$ is the number of ^{30}S ions injected, n is the number density of ^{4}He in the active target, ΔE is the energy bin size, $\Delta\Omega$ is the solid angle at a given energy bin, and m_α & $m_{^{30}\rm S}$ are the mass of ^{4}He & ^{30}S, respectively. Several of these quantities are quite trivial to determine, such as the atomic masses, the number of helium atoms in the target, yield of alpha particles, and energy binning employed. The number of injected ions are recorded for each run by a PPAC scaler, which can then be multiplied by the measured ^{30}S purity. The stopping power of ^{30}S in the active target fill gas was determined not only by the Bragg curves measured by the active target, but by measuring the residual ^{30}S ion energy with an SSD at various gas pressures; we found good agreement with Ziegler's method [16]. Finally, as the solid angle depends not only on the scattering depth but scattering position, we plotted the center-of-mass energy $E_{\rm cm}$ versus the center-of-mass solid angle $\Omega_{\rm cm}$ event-by-event and then fit it with an empirical function. The resulting excitation function is shown as the blue data points in Figure 2; the vertical errors are statistical, and the horizontal errors are from the binning of 100 keV (consistent with our achieved resolution mainly limited by the SSD).

To extract the parameters of the observed resonances, we used an R-Matrix formalism [17] computed via the SAMMY8 code [18]. The location of the resonance is determined by the resonance energy $E_{\rm r}$, the shape of the resonance from the angular momentum transfer ℓ, the height of the resonance from the alpha partial width Γ_α, and the width of the resonance from the total width Γ. The resonance energy $E_{\rm r}$ is just the elastic scattering center-of-mass energy $E_{\rm cm}$. As both nuclides in the entrance channel, ^{30}S and ^{4}He, have a spin-parity $J^\pi = 0^+$, then each ℓ value corresponds to a unique resonance $J^\pi_{\rm r}$ assignment in the compound nucleus ^{34}Ar as no orbital momentum can be transferred and the parity will always be natural. We can initially estimate Γ_α starting from the Wigner limit, and decreasing the width until the resonance height is matched. The total width Γ is the sum of the proton and alpha partial widths, as the gamma width is negligible in comparison so far above the particle thresholds. To estimate the proton width $\Gamma_{\rm p}$, we considered the spectroscopic factor θ_i^2 for each channel, and introduce a universal spectroscopic ratio ξ for the three resonances:

$$\begin{aligned} \theta_\alpha^2 &= \Gamma_\alpha / W_{\Gamma\alpha}, \\ \theta_{\rm p}^2 &= \Gamma_{\rm p} / W_{\Gamma p}, \\ \xi &\equiv \theta_{\rm p}^2 / \theta_\alpha^2, \\ \therefore \Gamma_{\rm p} &= \xi \theta_\alpha^2 W_{\Gamma p}. \end{aligned} \tag{2}$$

A similar approach was taken in the analysis of Ref. [19]. Two acceptable R-Matrix fits are shown in Figure 2 along with the case of pure Coulomb scattering (as no resonances were previously known in this energy region). The adopted level parameters are shown in Table 1, where we found the best fit for $\xi = 0.8\%$.

Table 1. Adopted level parameters for new states in ^{34}Ar along with calculations of the Wigner limit, derived from the best fit in Figure 2. The relationship between $E_{\rm r}$ and $E_{\rm ex}$ is the alpha threshold of 6.739 MeV for ^{34}Ar.

$E_{\rm r}$ (MeV)	$E_{\rm ex}$ (MeV)	ℓ_α	$J^\pi_{\rm r}$	Γ_α (keV)	$\Gamma_{\rm p}$ (keV)	θ^2_α %
4.35 ± 0.07	11.09 ± 0.07	2, 3	$(2^+, 3^-)$	$0.8^{+0.4}_{-0.4}$	1.3	15
4.75 ± 0.08	11.49 ± 0.08	2	2^+	12^{+6}_{-6}	9.7	30
5.52 ± 0.13	12.26 ± 0.13	1	(1^-)	290^{+0}_{-200}	65	> 99

As our new resonances are outside the XRB peak temperature 1–2 GK Gamow window, it is useful to include the preliminary results from RCNP [7] in a calculation of the ^{30}S$(\alpha, \rm p)$ stellar reaction rate.

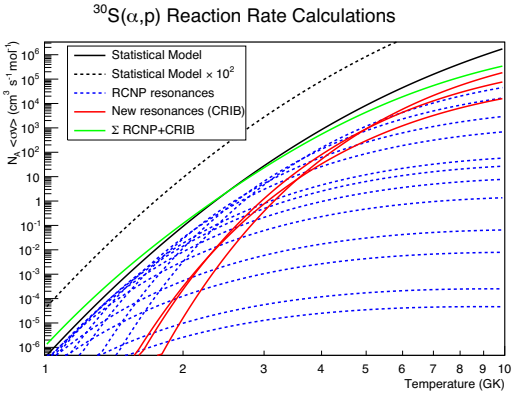

Figure 3. Calculations of the ^{30}S(α, p) stellar reaction rate from 1–10 GK. The statistical model (SM) rate from NON-SMOKER [20] is shown as the solid black line. The same SM rate artificially increased by a factor of 10^2 is shown as the black dashed line. The dashed blue lines represent 13 resonances from a preliminary report of an RCNP experiment [7], where we made many assumptions about their quantum properties. The solid red lines represent our higher-energy resonances with our best-fit quantum properties, shown also as the solid red line in Fig. 2. The sum of the RCNP and CRIB resonant contributions is shown in green.

However, the preliminary results from RCNP only provide us with rough resonance energies, and some assumptions are required. We assumed that each state has $J^\pi_r = 0^+$, and that $\Gamma_\alpha = \frac{1}{2}W_{\Gamma_\alpha}$. We also use the standard simplification that $\gamma = (\Gamma_\alpha\Gamma_p)/(\Gamma_\alpha + \Gamma_p) \approx \Gamma_\alpha$ when $\Gamma_\alpha \ll \Gamma_p$. The resulting resonance strength $\omega\gamma$ is constant within a factor of around two to three for $J \leq 3$ (although it quickly drops off for $J \geq 4$); this is because we parameterize the width based on the Wigner limit, which decreases with increasing J, where as for the ^{30}S+α entrance channel $\omega = 2J_r + 1$. While the contribution from an individual resonance calculated in this manner will be unreliable, the sum of these contributions can be considered an upper limit under an extreme assumption.

The calculated rates are plotted and compared against the NON-SMOKER [20] Hauser-Feshbach statistical model in Figure 3. The XRB model of the double-peaked structure required a reaction rate a factor of 10^2 greater than the statistical model to quench the proposed waiting point near ^{30}S [6]. Our new reaction rate evaluated with all known level structure of ^{34}Ar is inconsistent with a reaction rate deviating more than a factor of around 2 larger than the statistical model rate. The work demonstrates that while strong alpha resonances exist above the alpha-threshold in ^{34}Ar, they do not cause the stellar reaction rate to increase in a significant manner, vindicating the ^{30}S waiting point evidenced in many models assuming the statistical reaction rate.

4 Summary

We investigated the alpha-cluster structure of ^{34}Ar for the first time, using ^{30}S alpha resonant elastic scattering. Several new levels with large alpha-widths were discovered. However, we found that individual resonances with large alpha widths do not dominate the stellar reaction rate at XRB temperatures. This finding is contrary to the observation that in the lower mass regions, thermonuclear rates of (α, p) and (α, n) reactions on $T_z = \pm 1$ nuclei are dominated by isolated, alpha-cluster resonances, and we find that the statistical model may be considered an upper limit for $A \geq 30$ for such situations.

Acknowledgements

This experiment was conducted at the RI Beam Factory operated by the RIKEN Nishina Center and CNS, the University of Tokyo. This science could not be possible without the hard work and dedication from the RIKEN and CNS accelerator staff. The work was partly supported by JSPS KAKENHI (No. 21340053) from the Ministry of Education, Culture, Sports, Science, and Technology (MEXT) of Japan. We kindly acknowledge the above support and assistance.

References

[1] R.K. Wallace, S.E. Woosley, The Astrophysical Journal Supplement Series **45**, 389 (1981).
[2] A. Parikh, J. José, F. Moreno, C. Iliadis, The Astrophysical Journal Supplement Series **178**, 110. (2008)
[3] H. Schatz, K.E. Rehm, Nuclear Physics A **777**, 601 (2006).
[4] R.E. Taam, The Astrophysical Journal **241**, 358 (1980).
[5] C. Iliadis, P.M. Endt, N. Prantzos, W.J. Thompson, The Astrophysical Journal **524**, 434 (1999).
[6] J.L. Fisker, F.K. Thielemann, M. Wiescher, The Astrophysical Journal, Letters **608**, L61 (2004).
[7] S. O'Brien, T. Adachi, G.P.A. Berg, M. Couder, M. Dozono, H. Fujita, Y. Fujita, J. Görres, K. Hatanaka, D. Ishikawa et al., American Institute of Physics Conference Series **1090**, 288 (2009)
[8] C.M. Deibel, K.E. Rehm, J.M. Figueira, J.P. Greene, C.L. Jiang, B.P. Kay, H.Y. Lee, J.C. Lighthall, S.T. Marley, R.C. Pardo et al., Physical Review C **84**, 045802 (2011).
[9] K.P. Artemov, O.P. Belyanin, A.L. Vetoshkin, R. Wolskj, M.S. Golovkov, V.Z. Gol'dberg, M. Madeja, V.V. Pankratov, I.N. Serikov, V.A. Timofeev et al., Soviet Journal of Nuclear Physics **52**, 408 (1990).
[10] S. Kubono, Y. Yanagisawa, T. Teranishi, S. Kato, Y. Kishida, S. Michimasa, Y. Ohshiro, S. Shimoura, K. Ue, S. Watanabe et al., European Physical Journal A **13**, 217 (2002).
[11] Y. Yanagisawa, S. Kubono, T. Teranishi, K. Ue, S. Michimasa, M. Notani, J.J. He, Y. Ohshiro, S. Shimoura, S. Watanabe et al., Nuclear Instruments and Methods in Physics Research A **539**, 74 (2005).
[12] H. Yamaguchi, Y. Wakabayashi, G. Amadio, S. Hayakawa, H. Fujikawa, S. Kubono, J.J. He, A. Kim, D.N. Binh, Nuclear Instruments and Methods in Physics Research A **589**, 150 (2008).
[13] D. Kahl, A.A. Chen, S. Kubono, D.N. Binh, J. Chen, T. Hashimoto, S. Hayakawa, D. Kaji, A. Kim, Y. Kurihara et al., American Institute of Physics Conference Series **1213**, 208 (2010).
[14] H. Kumagai, A. Ozawa, N. Fukuda, K. Sümmerer, I. Tanihata, Nuclear Instruments and Methods in Physics Research A **470**, 562 (2001).
[15] D. Kahl, T. Hashimoto, N.N. Duy, S. Kubono, H. Yamaguchi, D.N. Binh, A.A. Chen, S. Cherubini, S. Hayakawa, J.J. He et al., American Institute of Physics Conference Series **1594**, 163 (2014).
[16] J.F. Ziegler, J.P. Biersack, M.D. Ziegler, *SRIM - The Stopping and Range of Ions in Matter* (Lulu Press, 2012).
[17] A.M. Lane, R.G. Thomas, Reviews of Modern Physics **30**, 257 (1958).
[18] N. Larson (2000), ORNL/TM-9179/R5 (Unpublished).
[19] D.N. Binh, Ph.D. thesis, The University of Tokyo (2010).
[20] T. Rauscher, F.K. Thielemann, Atomic Data and Nuclear Data Tables **79**, 47 (2001).